Electronic Supplementary Information

The Dechlorination of Chlorobenzene on Vanadium-based Catalysts for Low-temperature SCR

Dong Wang, Jian-jun Chen, Yue Peng*, Wen-zhe Si, Xian-sheng Li, Bing Li, Jun-hua

Li*

[1]*State Key Joint Laboratory of Environment Simulation and Pollution Control, School

of Environment, Tsinghua University, Beijing 100084, China*

*Corresponding author.

Phone: +86 010 62771093

E-mail address: pengyue83@tsinghua.edu.cn (Yue Peng), lijunhua@tsinghua.edu.cn (Jun-hua

Li)

1. Experimental

1.1. Catalyst preparation

The catalysts were prepared according to conventional commercial catalyst preparation methods with pilot scale (Mixing-Extrusion molding-Drying-Calcining). Vanadium was used as the main active component (5 w.t.%), and a certain amount of manganese (4 w.t.%) or cerium (4 w.t.%) was added. The molding samples were crushed and sieved to a size of 40 - 60 mesh for test. The samples were denoted as VC, Ce-VC and Mn-VC where VC represents vanadium-based catalyst.

1.2. Catalyst characterization

Diffuse reflectance infrared Fourier transform spectroscopy (DRIFTS) experiments were performed on a FTIR spectrometer (ThermoFisher, Nicolet NEXUS 6700) equipped with a Harrick IR cell and MCT/A detector cooled by liquid nitrogen. Prior to each experiment, the catalyst was preheated at 350 °C for 1 h with N_2 at a flow of 100 mL·min^{-1}. All of the in situ DRIFTS spectra were recorded by accumulating 64 scans with a resolution of 4 cm^{-1}.

The temperature-programmed desorption of NH_3 (NH_3-TPD) was performed in a fixed-bed quartz reactor using an FTIR spectrometer detector (MKS, MultiGas 2030HS). The samples were first pretreated at 500 °C for 1 h in N_2 and then cooled down to 100 °C. After that, the samples were (exposed to 50 ppm C_6H_5Cl/N_2 for 1 h when pretreated with CB) exposed to 500 ppm NH_3/N_2 for 1 h at 100 °C until adsorption equilibrium, followed by N_2 purge for another 1 h at 100 °C. Finally, the temperature programed desorption was run to 780 °C in N_2 flow with heating rate of

10 °C·min^{-1}.

The chromatographic system was 761 Compact IC (Metrohm, Switzerland) equipped with a conductivity detection. The separation was performed on an Metrosep A sup 5 anion separation column. The system was operated under isocratic mode of carbonate (3.2 mmol·L^{-1} Na$_2$CO$_3$ + 1.0 mmol·L^{-1} NaHCO$_3$).

The desorption of the targets retained on the vanadium-based catalysts was carried out on a CDS 7500S Thermal Desorption System (CDS Analytiacl, USA). Prior to thermal desorption, the tubes were purged at 40 °C for 1 min, and then heated to 300 °C and held for 5 min to desorb and then focused into a cold trap. The cold trap was rapid heated to 300 °C for 3 min to release the targets into GC-MS system (7890B GC/5977B MSD system, Agilent Technologies, Santa Clara, CA, USA). The analytes was separated on a DB-5MS capillary column (30 m×0.32 mm×1.0 μm, 5% phenyl /95 % dimethylpolysiloxane, J&W Scientific, USA). The GC oven temperature was initially held at 35 °C for 5 min, increased to 300 °C at the rate of 10 °C min^{-1} for 5 min. The ion source and quadrupole temperatures were set at 230 °C and 200 °C, respectively. Samples were monitored in the scanning range of 45 - 500 (m/z).

Thermal desorption (TD) was carried out on an CDS 7500S (CDS Analytiacl, USA). Helium was used as the desorption gas to direct the desorbed organic compounds to the GC injection port. TD tubes were screw-mounted with a GC injection needle. TD started 1.0 min after the needle was inserted through the GC septum into heated GC inlet (250 °C) for pressure stabilization. When desorption was

completed, the cryo-trap was held at − 20 °C for an additional 0.5 min to prevent pressure fluctuations, after which time, the GC/MS program started and the cryo-trap was heated at about 10 °C·min^{-1} from 35 to 300 °C. The TD device was connected to an Agilent GC 7890B coupled with an Agilent 5977B MS detector (Agilent, Santa Clara, CA, USA). The ion source and quadrupole temperatures were set at 230 °C and 200 °C, respectively. Samples were monitored in the scanning range of 45 - 500 (m/z).

N$_2$ adsorption-desorption isotherms over catalysts were obtained at -196 °C using Micromeritics TriStar II 3020 Surface Area and Porosity Analyzer. Prior to N$_2$ physisorption, the catalysts were degassed at 300 °C for 8 h. Average pore diameters, pore volumes and pore size distributions were determined by Barrett-Joyner-Halenda (BJH) method from the desorption branches of the isotherms. Surface areas were determined by Brunauer-Emmertt-Teller (BET) equation in 0.05 - 0.35 partial pressure range. Textural properties of micropores were calculated using t-plot model.

The chemical states of surface compositions were observed by X-ray photoelectron spectra (XPS) recorded using a Thermo ESCALAB 250XI photoelectron spectrometer. Test conditions were: Mono Al ka, hv =1486.6 eV, 150 W, 500 μm. Binding energies were calibrated using C 1s (BE=184.8 eV) as a standard.

The crystalline phase of catalysts was measured by powder X-ray diffraction (XRD) using a Bruker D8 Advance diffractometer with a nickel filter operating at 40 kV and 40 mA in the 2θ range of 5 - 80 ° at a scanning rate of 4 °·min^{-1}. The diffraction lines were identified by matching with reference patterns in the JCPDS database.

Temperature programmed desorption of oxygen (O_2-TPD) was carried out in a conventional apparatus equipped with TCD. The samples were pretreated at 300 °C for 1 h, and then cooled to 40 °C. The adsorption of O_2 was operated at 40 °C with pure oxygen (30 mL·min^{-1}) for 30 min. After that, the samples were purged with He until the base line remained unchanged. Finally, the samples were heated at a rate of 10 °C·min^{-1} to 800 °C.

1.3. Catalyst activity measurement

The SCR activity were measured in a fixed-bed quartz reactor. The test was carried out under atmospheric pressure at the temperature range of 100-300 °C. The total flow rate was 100 mL·min^{-1} responding to the GHSV of 60,000·mL·g^{-1}·h^{-1}. The typical reactant gas composition was as follows: 500 ppm NH_3, 500 ppm NO, 3.5 vol. % O_2, 50 ppm C_6H_5Cl (when used) and balance N_2. The concentrations of the gases (NO, NO_2, N_2O, C_6H_5Cl, CO_2 and NH_3) were continually monitored by an FTIR spectrometer (Gasmet FTIR DX-4000). And the data was recorded only when the reaction reached the steady state after 30 minutes of continuous and stable operation running at each measuring temperature. Then, the NO_x conversion (η_1) and C_6H_5Cl conversion (η_2) were calculated according to the following equations:
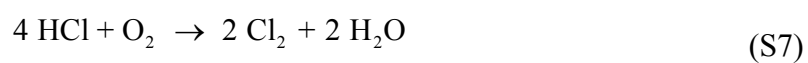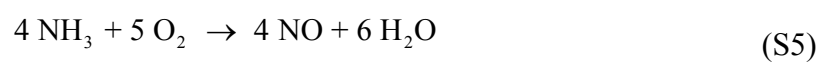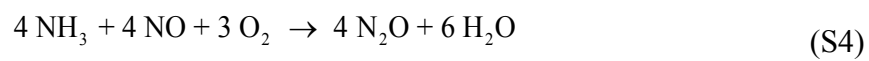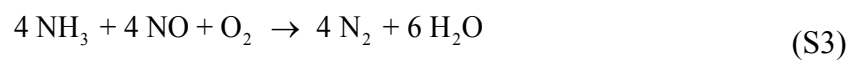
$$\eta_1 = \frac{[NO_x]_{in} - [NO_x]_{out}}{[NO_x]_{in}} \times 100\%$$

(S1)

$$\eta_2 = \frac{[C_6H_5Cl]_{in} - [C_6H_5Cl]_{out}}{[C_6H_5Cl]_{in}} \times 100\%$$

(S2)

where $[NO_x]_{in}$ and $[NO_x]_{out}$ were the concentrations of gaseous NO_x in the inlet and outlet, respectively. The gaseous C_6H_5Cl were expressed the same way. NO_x included

NO and NO_2.

1.4. Reaction equations

$$4\,NH_3 + 4\,NO + O_2 \ \rightarrow\ 4\,N_2 + 6\,H_2O \tag{S3}$$

$$4\,NH_3 + 4\,NO + 3\,O_2 \ \rightarrow\ 4\,N_2O + 6\,H_2O \tag{S4}$$

$$4\,NH_3 + 5\,O_2 \ \rightarrow\ 4\,NO + 6\,H_2O \tag{S5}$$

$$C_6H_5Cl \ \rightarrow\ C_6H_5{}^{\oplus} + Cl^{\otimes} \tag{S6}$$

$$4\,HCl + O_2 \ \rightarrow\ 2\,Cl_2 + 2\,H_2O \tag{S7}$$

Caption to Tables

Table 1S.   Textural properties of the vanadium-based catalysts.

Table 2S.   Textural properties of the vanadium-based catalysts.

Table 3S.   Detailed data of benzene series on the catalysts by purge and trap-thermal desorption

gas chromatography-mass spectrometry.

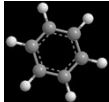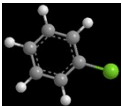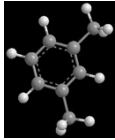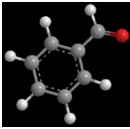Table 1S.   Textural properties of the vanadium-based catalysts.
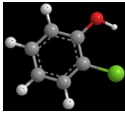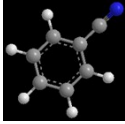
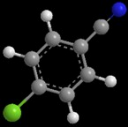| Samples	S_{BET} /m^2·g^{-1}	Pore volume /cm^3·g^{-1}	Average Pore diameter /nm
Mn-VC	57.8786	0.289146	15.2819
Ce-VC	63.9914	0.339236	16.5680
VC	50.3154	0.270299	16.3127

Table 2S.　Textural properties of the vanadium-based catalysts.

Samples	t-Plot Micropore Area /m²·g⁻¹	t-Plot External Surface Area /m²·g⁻¹	t-Plot Micropore Volume /cm³·g⁻¹
Mn-VC	25.7333	32.1453	0.006599
Ce-VC	28.5184	35.4729	0.007254
VC	21.1900	29.1254	0.005463

Table 3S. Detailed data of benzene series on the catalysts by purge and trap-thermal desorption gas chromatography-mass spectrometry.

Species	Pretreatment	Samples	m/z	RT	Area	Area % [a]	Area Total %
Benzene (C_6H_6)	NH$_3$	VC	78.1	3.291	13552251.34	23.16	4.26
		Ce-VC	78.1	3.296	17389884.69	18.57	4.05
		Mn-VC	78.1	3.291	13152087.11	50.97	4.83
	CB	VC	78.1	3.288	14496226.06	6.86	1.9
		Ce-VC	78.1	3.286	18651404.27	87.68	8.02
		Mn-VC	78.1	3.286	11516153.99	57.78	4.74
Benzene, chloro- (C_6H_5Cl)	NH$_3$	VC	112	7.919	13404464.3	22.91	4.21
		Ce-VC	112	7.919	3651157.51	3.9	0.85
		Mn-VC	112	7.919	1816507.36	7.04	0.67
	CB	VC	112	7.92	4353525.93	2.06	0.57
		Ce-VC	112	7.92	7254483.4	34.1	3.12
		Mn-VC	112	7.92	2683424.23	13.46	1.1
Benzene, 1, 3-dimethyl- (C_8H_{10})	NH$_3$	VC	91.1	8.516	316582.81	0.54	0.1
		Ce-VC	91.1	8.519	639183.55	0.68	0.15
		Mn-VC	91.1	8.52	358705.12	1.39	0.13
	CB	VC	-	-	-	-	-
		Ce-VC	91.1	8.517	474555.2	2.23	0.2
		Mn-VC	91	8.517	250937.68	1.26	0.1
Benzaldehyde (C_7H_6O)	NH$_3$	VC	106.1	10.669	581312.72	0.99	0.18
		Ce-VC	106.1	10.666	1547932.17	1.66	0.36
		Mn-VC	105	10.67	397680.8	1.54	0.14
	CB	VC	-	-	-	-	-
		Ce-VC	106	10.667	2535566.39	11.92	1.09
		Mn-VC	106.1	10.667	747562.27	3.75	0.31
Phenol, 2-chloro- (C_6H_5ClO)	NH$_3$	VC	128	11.227	14008906.33	23.94	4.4
		Ce-VC	128	11.227	3120282.94	3.33	0.73
		Mn-VC	128	11.228	474226.96	1.84	0.17
	CB	VC	128	11.231	2199655.77	1.04	0.29
		Ce-VC	128	11.227	4060194.8	19.09	1.75
		Mn-VC	128	11.227	1405707.95	7.05	0.58
Benzonitrile (C_7H_5N)	NH$_3$	VC	103.1	11.128	58515096.46	100	18.38
		Ce-VC	103.1	11.112	10163309.91	10.85	2.37
		Mn-VC	103.1	11.112	13450792.49	52.12	4.94

		VC	103.1	11.123	47430384.42	22.43	6.21
	CB	Ce-VC	103	11.112	12055796.8	56.67	5.19
		Mn-VC	103.1	11.112	15543635.7	77.98	6.4
Benzonitrile, 2/4-chloro- (C₇H₄ClN)	NH₃ pretreated	VC	137.1	14.007	388533.1	0.75	0.14
		Ce-VC	-	-	-	-	-
		Mn-VC	137	14.005	786224.8	3.05	0.29
	CB pretreated	VC	137.1	13.744	26877643.25	12.71	3.52
		Ce-VC	137	13.742	239536.25	1.13	0.1
		Mn-VC	137	14	8383579.63	42.06	3.45

[a] the percentage of the characteristic peak area to the maximum characteristic peak area.

Caption to Figures

Figure 1S.

a: Pore size distributions of the vanadium-based catalysts.

b: Cumulative pore volumes of the vanadium-based catalysts.

Figure 2S.

N_2 adsorption-desorption isotherms of the vanadium-based catalysts
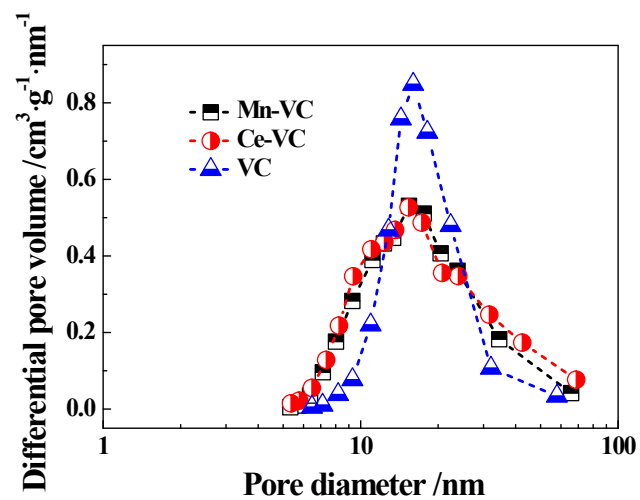
a: Mn-VC

b: Ce-VC

b: VC

Figure 3S.

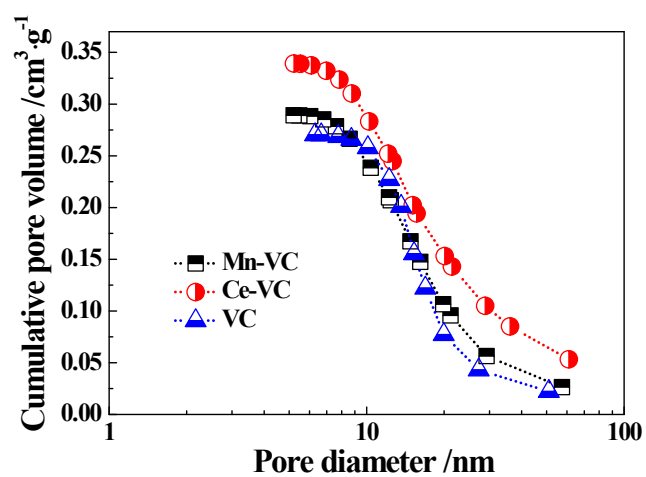XPS spectra of the vanadium-based catalysts over the spectral regions of O 1s.

Figure 4S.

XRD patterns of the vanadium-based catalysts.

Figure 5S.

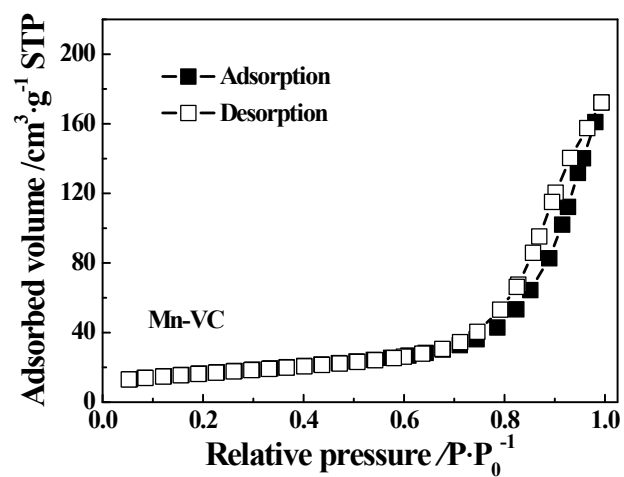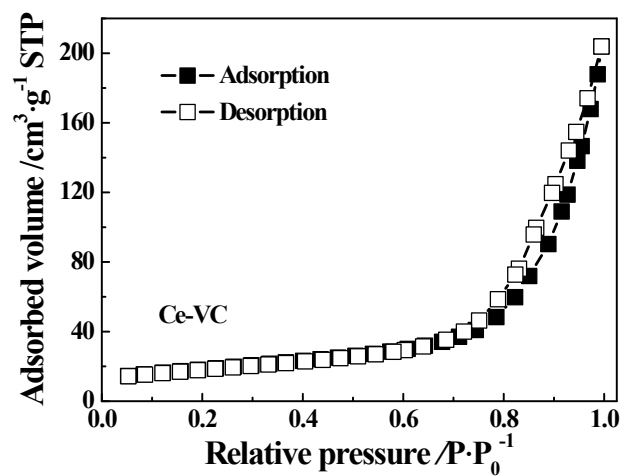O_2-TPD (b) profiles of the vanadium-based catalysts.

(a)

(b)

Figure 1S.

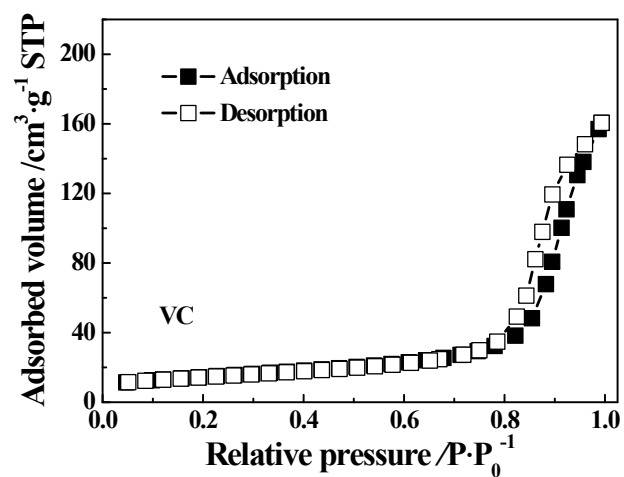a: Pore size distributions of the vanadium-based catalysts.

b: Cumulative pore volumes of the vanadium-based catalysts.

(a)

(b)

(c)

Figure 2S.

N_2 adsorption-desorption isotherms of the vanadium-based catalysts.

a: Mn-VC

b: Ce-VC

b: VC

Figure 1S b shows the cumulative pore volumes of catalysts. It can be observed that Ce-WV exhibits the highest cumulative pore volume as showed in **Table 1S**. The three catalysts show the highest cumulative rate at the pore diameter range of 10-30 nm.

Nitrogen adsorption-desorption isotherms for catalysts are shown in **Figure 2S**. For the three catalysts, the isotherm resembles closely with type V isotherm according to the IUPAC classification, which is typical for mesoporous materials. In addition, the hysteresis loops exhibit a shape of typical H3 type, revealing the exist of the slit-shaped pore structures in the catalysts. The interaction between catalysts and N_2 is weak under low pressure. When the relative pressure (the ratio of N_2 pressure and saturated vapor pressure of N_2 under the adsorption temperature) is 0, all the catalysts show slight N_2 adsorption volume (less than 10 $cm^3 \cdot g^{-1}$) . This shows that there is almost no micropore (with the pore diameter < 2 nm) in the catalysts. When the relative pressure >0.8, the N_2 adsorption volume rises steeply, causing by condensation of N_2 in the mesoporous (with the pore diameter range of 2-50 nm) and macroporous (with the pore diameter >50 nm). It can be speculated that the vanadium-based catalysts contains a considerable number of mesoporous and macroporous. The closure points of hysteresis loops for Mn-VC, Ce-VC and VC are at P/P_0 of 0.68, 0.64 and 0.75, respectively. The greater the relative pressure for the closure point of hysteresis loop is, the more large pores exist. Therefore, the VC shows more large pore structures.

The experimental data of N_2 isothermal adsorption-desorption over the vanadium-based catalysts were further processed with the T-Plot model, and the results are shown in **Table 2S**. There is not much microporous structures in these catalysts. This can also be concluded by their

micropore volume being close to 0. The main pore structures of maghemite catalyst are
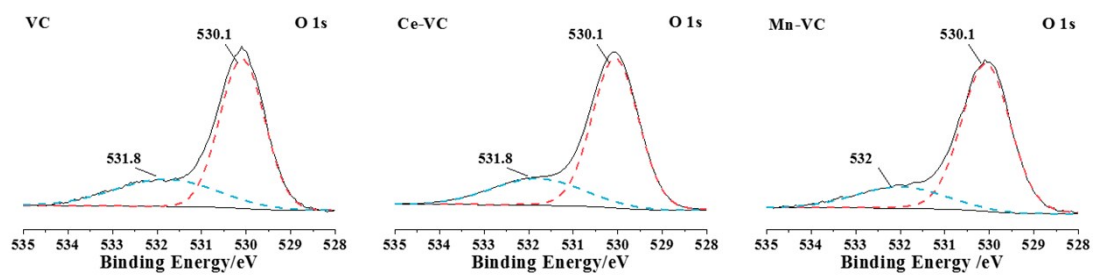
mesoporous.

Figure 3S.

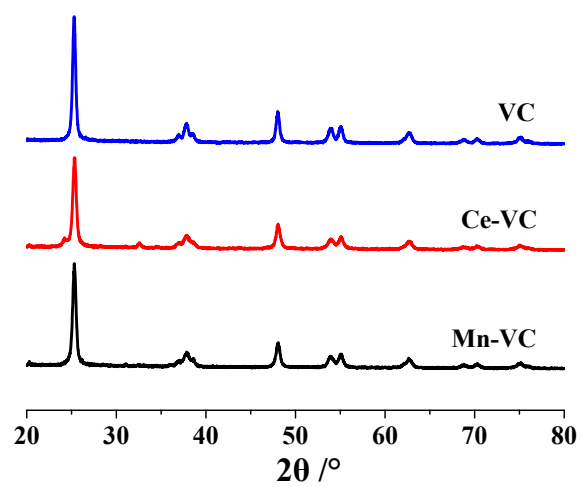XPS spectra of the vanadium-based catalysts over the spectral regions of O 1s.
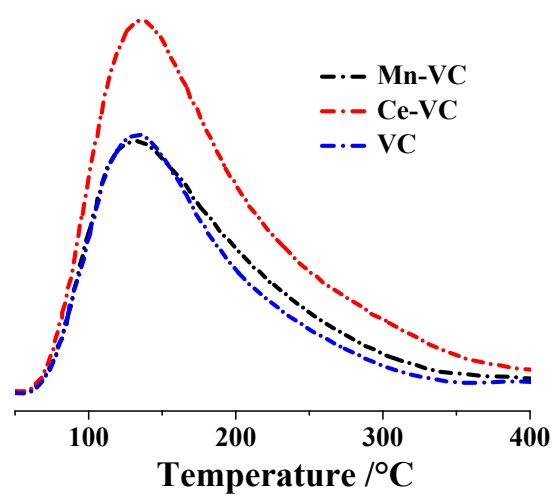
Figure 4S.

XRD patterns of the vanadium-based catalysts.

Figure 5S.

O$_2$-TPD (b) profiles of the vanadium-based catalysts.

References

[S1] Yang, S.; Liao, Y.; Xiong, S.; Qi, F.; Dang, H.; Xiao, X.; Li, J., N_2 selectivity of NO reduction by NH_3 over MnO_x-CeO_2: Mechanism and key factors. *J. Phys. Chem. C* **2014,** *118*, 21500-21508.

[S2] Chmielarz, L.; Kustrowski, P.; Rafalska-Lasocha, A.; Dziembaj, R., Selective oxidation of ammonia to nitrogen on transition metal containing mixed metal oxides. *Appl. Catal. B-environ* **2005,** *58*, 235-244.

[S3] Topsoe, N. Y., Mechanism of the selective catalytic reduction of nitric oxide by ammonia elucidated by in situ online Fourier transformation infrared spectroscopy. *Science* **1994,** *265*, 1217-1219.

[S4] Long, R. Q.; Yang, R. T., Selective catalytic oxidation of ammonia to nitrogen over Fe_2O_3-TiO_2 prepared with a sol-gel method. *J. Catal.* **2002,** *207*, 158-165.

[S5] Zhang, Y. P.; Zhu, X. Q.; Shen, K.; Xu, H. T.; Sun, K. Q.; Zhou, C. C., Influence of ceria modification on the properties of TiO_2-ZrO_2 supported V_2O_5 catalysts for selective catalytic reduction of NO by NH_3. *J.Colloid Interf. Sci.* **2012,** *376*, 233-238.

[S6] Busca, G.; Lietti, L.; Ramis, G.; Berti, F., Chemical and mechanistic aspects of the selective catalytic reduction of NO_x by ammonia over oxide catalysts: A review. *Appl. Catal. B-environ* **1998,** *18*, 1-36.

[S7] Wang, Z.; Qu, Z. P.; Quan, X.; Wang, H., Selective catalytic oxidation of ammonia to nitrogen over ceria-zirconia mixed oxides. *Appl. Catal. A -gen* **2012,** *411*, 131-138.

[S8] Yang, S. J.; Li, J. H.; Wang, C. Z.; Chen, J. H.; Ma, L.; Chang, H. Z.; Chen, L.; Peng, Y.; Yan, N. Q., Fe-Ti spinel for the selective catalytic reduction of NO with NH_3: Mechanism and structure-activity relationship. *Appl. Catal. B-environ* **2012,** *117*, 73-80.

[S9] Jung, S. M.; Grange, P., DRIFTS investigation of V=O behavior and its relations with the reactivity of ammonia oxidation and selective catalytic reduction of NO over V_2O_5 catalyst. *Appl. Catal. B-environ* **2002,** *36*, 325-332.